

## Effect of Annealing on Microstructure and Magnetic Properties of Mn Ferrite Powder

Amit S. Bandekar<sup>1</sup>, Paresh S. Gaikar<sup>2</sup>, Ankita P. Angre<sup>3</sup>, Aishwarya M. Chaughule<sup>4</sup> & Nana S. Pradhan<sup>1\*</sup>

<sup>1</sup>Department of Physics, Ramnarain Ruia Autonomous College, Matunga, Mumbai, 400019, INDIA

<sup>2</sup>Department of Physics, Mahatma Phule A. S. C. College, Panvel, Raigad, 410206, INDIA

<sup>3</sup>Department of Physics, Satish Pradhan Dnyanasadhana College, Thane, 400604, INDIA

<sup>4</sup>Department of Physics, Andhra College, Wadala Mumbai, 400031, INDIA

\* Correspondence: E-mail: [amitbandekar78@gmail.com](mailto:amitbandekar78@gmail.com)

(Received 10 Dec, 2018; Accepted 11 Jan, 2019; Published 18 Jan, 2019)

**ABSTRACT:** Mn ferrite powder ( $\text{MnFe}_2\text{O}_4$ ) were prepared by the wet chemical co-precipitation method and after-ward annealed in air. The effects of heat treatment temperature on crystalline phases formation, microstructure and magnetic properties of  $\text{MnFe}_2\text{O}_4$  were investigated by X-ray diffraction, Fourier-transform infrared spectroscopy, Scanning Electron Microscopy and SQUID. All annealed sample showed pure ferrite phase, larger saturation magnetization was observed at  $900^\circ\text{C}$  ( $M_s = 75.1 \text{ emu/g}$ ) and lower coercivity ( $H_c = 33.04 \text{ Oe}$ ) compared with the co-precipitated ferrite powder at  $700^\circ\text{C}$  ( $M_s = 44.32 \text{ emu/g}$ ,  $H_c = 62.6 \text{ Oe}$ ). The  $600^\circ\text{C}$  air-annealed sample had the largest blocking temperature ( $T_b = 10.88 \text{ K}$ ). Field-dependent magnetization measurements show low coercivities with no remanence giving additional proof for the superparamagnetic behavior. It is also observed that with increasing annealing temperature the  $T_c$  value also increases.

**Keywords:** Ferrite; Chemical co-precipitation; Crystalline; Magnetization; Microstructure;  $\text{MnFe}_2\text{O}_4$ ; Superparamagnetic.

**INTRODUCTION:**  $\text{MnFe}_2\text{O}_4$  has the highest permeability and saturation induction of the ferrite class of materials and has the advantage of various stoichiometries with nearly zero magneto-crystalline anisotropy and magneto-restriction, important for stress insensitivity and low noise.  $\text{MnFe}_2\text{O}_4$  are very important soft magnetic materials because of their high initial magnetic permeability, saturation magnetization, electrical resistivity and low power losses [1,2]. Mn ferrites are very important in biomedicine as magnetic carriers for bioseparation, enzymes and proteins immobilization [3–6]. Additionally, These materials are extensively used as inductors, transformers, antenna rods, loading coils, deflection yokes, choke coils, recording heads, magnetic amplifiers, electromagnetic interference devices (EMI), power transformers and splitters [7,8]. Recently, with the development of greater frequency, small power miniaturized electronic devices, special focus has been placed on the preparation of high-performance Mn ferrite powders. To prepare high electromagnetic performance  $\text{MnFe}_2\text{O}_4$ , various synthesizing methods have been reported recently, including alcohol dehydration, spray drying, hydrothermal synthesis, and sol-gel methods [9–13]. However, these methods are econom-

ically unfeasible for large-scale production. Recently more attention has been paid to the co-precipitation method, which permits producing ultra-fine powders with chemically homogeneous composition, uniform size and good reactivity [14,15]. The advantages of this method are processing simplicity, extraordinary production efficiency, small energy loss, and high-purity products. In this present work,  $\text{MnFe}_2\text{O}_4$  powders were prepared by the wet chemical co-precipitation method. Then the as-prepared powders were annealed at different temperatures range  $600$  to  $900^\circ\text{C}$  for 3h in the air. Afterwards, Structural and magnetic properties of annealed  $\text{MnFe}_2\text{O}_4$  were explored.

**EXPERIMENTAL:** To prepare nanoparticles, the required amount of Manganese chloride and Ferric chloride were taken in the molar ratio of 1:2 and dissolved in a suitable volume of double distilled water. Thereafter, preheated sodium hydroxide was added to this solution until the pH value of the solution was maintain pH value ( $\text{pH} > 12$ ), as it plays an important role in controlling the precipitation and size of the precipitate particles. The solution was heated up to  $80^\circ\text{C}$ . The solution was stirred continuously and al-

lowed to cool down up to room temperature slowly. Afterwards, the resulting fluid centrifuged at 3000 rpm for about 10 minutes. Then centrifuged precipitate settled down at the bottom. The supernatant of the fluid was discarded. The precipitate so obtained, was taken out then washed with double distilled water. The synthesized product was then dried at room temperature for 24 hours. The co-precipitated ferrite was then grinded using a pestle to have very fine particles.

In order to examine the influence of annealing temperature on structural and magnetic properties of  $MnFe_2O_4$  powders were annealed at 600, 700, 800 and 900°C respectively for 3h in the air. X-ray diffraction (XRD) was used to determine the phases and crystalline size of samples. XRD plots were recorded on a Rigaku Ultima IV diffractometer in the range between 10 and 80° using graphite-monochromated Cu K $\alpha$  radiation ( $\lambda = 0.15418$  nm) at 40 kV accelerating voltage with 40 mA current. The infrared spectra for all the compositions were measured in the wave number range of 4000 – 400  $cm^{-1}$ , using Shimadzu IR PRESTIGE-21 FT-IR spectrometer at Dr. P. S. Ramanathan Advanced Instrumentation Centre, Ramnarain Ruia College, and Matunga. Size of particles and morphologies were observed by scanning electron microscopy (SEM) (FESEM INSPECT F50). Quantum Design MPMS-XL SQUID was used for magnetic properties study. Properties of particles were investigated by standard zero-field-cooling (ZFC) and field cooling (FC) procedures. The applied magnetic field was 512 Oe and the temperature range was from 2 K to 380 K.

## RESULT AND DISCUSSION:

**Phase analysis:** The XRD patterns of the  $MnFe_2O_4$  nanoparticles calcined at different temperature are shown in Figure 1. The patterns show the reflection planes (1 1 1), (2 2 0), (3 1 1), (2 2 2), (4 0 0), (4 2 2), (5 1 1), (4 4 0), and (5 3 1), which confirm the presence of single phase  $MnFe_2O_4$  with a face-centered cubic structure which is matched with standard JCPDS file no. 10-0319[16], showing that the prepared ferrites are pure. Fig. 1 shows the effect of the annealing temperature on the crystalline sizes of the annealed  $MnFe_2O_4$  powders. The average crystalline sizes were determined using the famous Debye-Scherrer's formula [17]. The crystalline size of the  $MnFe_2O_4$  powder increases from 18.88 to 21.57 nm with the annealing temperature increase from 700 to 900°C and its maximum value is 34.98 nm at 600°C.

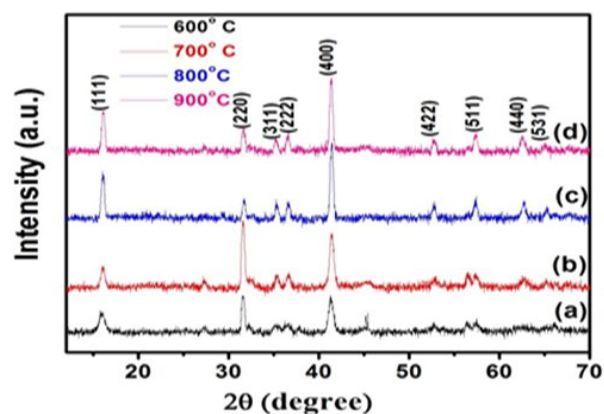


**Figure 1:** XRD patterns of manganese ferrite nanoparticles annealed at different temperatures.

**FT-IR Spectroscopy:** The infrared (IR) absorption spectra were recorded in the wave number range 400–4000  $cm^{-1}$ . The  $MnFe_2O_4$  samples were studied further for the crystalline  $MnFe_2O_4$  nanostructures at different annealed temperatures using FT-IR spectra analysis (Figure 2). The FT-IR spectra demonstrate that absorption bands of Mn–O and Fe–O bonds appeared at 469 and 504  $cm^{-1}$  respectively, for inverse spinel  $MnFe_2O_4$  that was annealed at 700°C. These bonds provide evidence the formation of the metal ions oxygen in the tetrahedral and octahedral sites in the spinel structure, as suggested by previously published data [18]. At the 700°C, however, there were still traces of broadband absorption peaks due to traces of adsorbed or atmospheric  $CO_2$  and O–H stretching vibration [19].

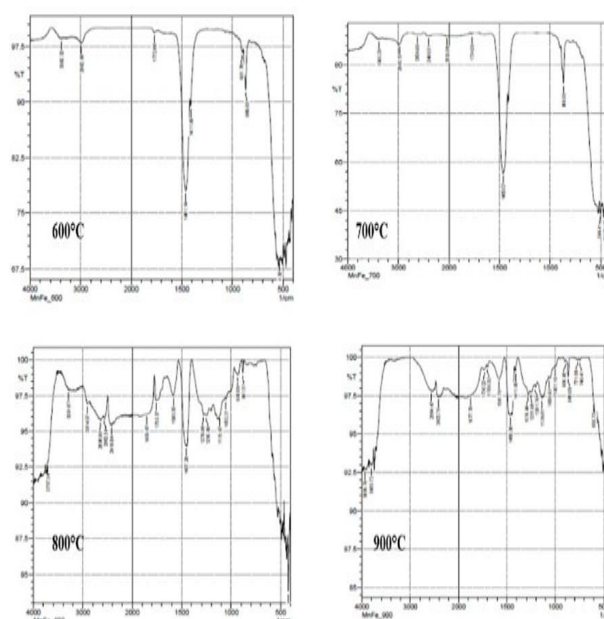


**Figure 2:** FT-IR spectra of  $MnFe_2O_4$  annealed at a different temperature.

**Microstructure evolution with annealing temperature:** The scanning electron micrographs (SEM) for  $\text{MnFe}_2\text{O}_4$  annealed at different temperature (Temp. = 600°C, 700°C, 800°C and 900°C) are displayed in Figure 3. It can be seen that the grain size becomes larger with the rise of annealing temperature. This nature of SEM suggests that, several neighboring particles fuse together to increase particle sizes by melting their surfaces [20]. This grain growth of particle size enlargement at higher annealed temperatures has been observed previously in manganese ferrite [21], cobalt ferrite [22] and in zinc ferrite [23] systems.

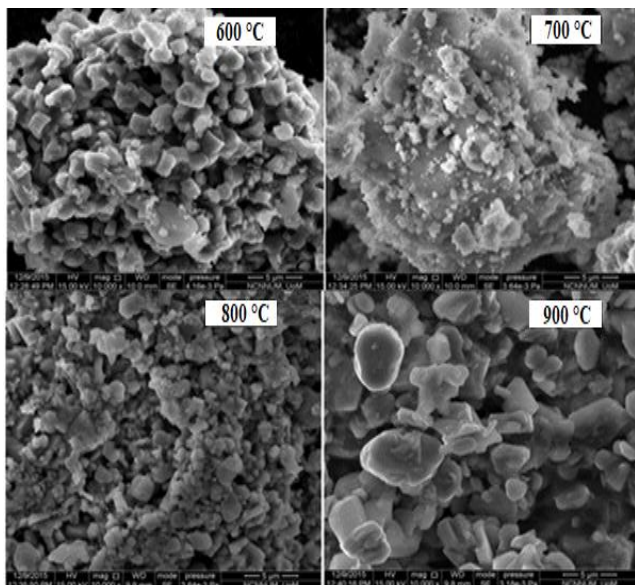


**Figure 3: Scanning electron micrographs for  $\text{MnFe}_2\text{O}_4$  annealed at in the temperature range 600-900°C.**

**Magnetic properties:** Particles size and shape may strongly affect their resultant magnetic behavior and it has been detected how these characteristic vary depending on the annealing temperature, this section is focused on studying the magnetic behaviors chemically co-precipitated  $\text{MnFe}_2\text{O}_4$  particles annealed at a different temperature in air. Figure 4 shows the curves of magnetization of precursor and  $\text{MnFe}_2\text{O}_4$  nanoparticles which revealed a typical super-paramagnetic behavior. Table 1 depicts the values of saturation magnetization ( $M_s$ ) of different samples for  $\text{MnFe}_2\text{O}_4$  nanoparticles.

When the annealing temperature increased from 600°C to 900 °C, the saturation magnetization increased from 24 to 73 emu/g. This can be attributed to spin canting and surface spin disorder that occurred in these nanoparticles [24]. The interactions between the A and B sub-lattices in the spinel lattice system ( $\text{AB}_2\text{O}_4$ ) consist of inter-sub-lattice (A-B) super-exchange interactions and intra-sub-lattice (AA) and

(B-B) exchange interactions. Inter-sub-lattice super-exchange interactions of the cations on the (A-B) are much stronger than the (A-A) and (B-B) intra-sub-lattice exchange interactions [25, 26].

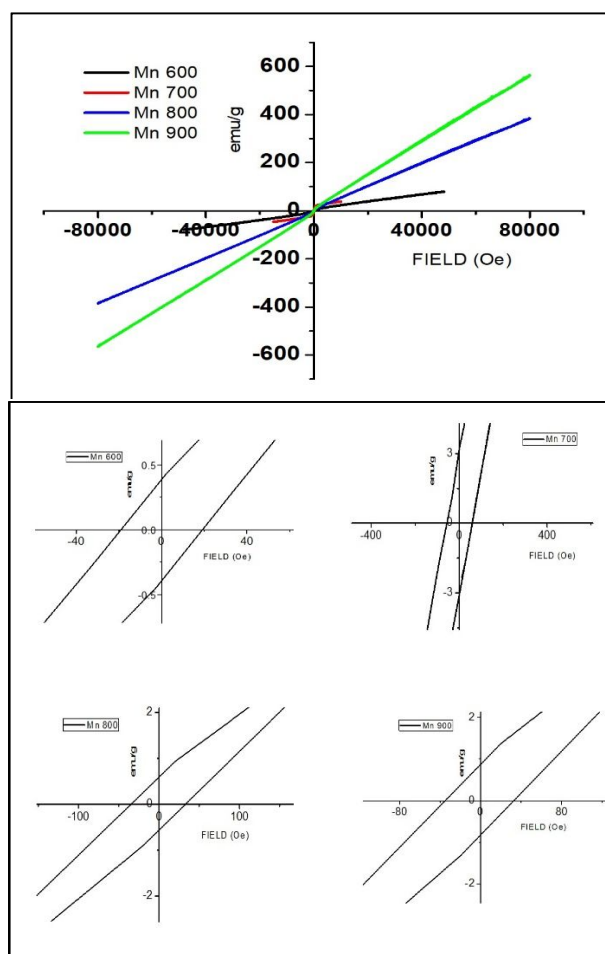


**Figure 4: The magnetization curves of the  $\text{MnFe}_2\text{O}_4$  nanoparticles annealed at a different temperature which measured at room temperature and the expanded field region around the origin for clear visibility of the readers.**

The temperature dependence of the magnetization was measured using zero field cooling and field cooling (ZFC– FC) procedures from 2 to 300 K in an applied field of 512 Oe (Figure 5). With growing temperature the ZFC magnetization grows, before reaching a maximum value, i.e., the blocking temperature  $T_B$ , at about 10.88 K for  $\text{MnFe}_2\text{O}_4$  annealed at 600°C, 7.96 K for  $\text{MnFe}_2\text{O}_4$  annealed at 700°C, 8.35 K for  $\text{MnFe}_2\text{O}_4$  annealed at 800°C and 6.82 K for  $\text{MnFe}_2\text{O}_4$  annealed at 900°C. At temperatures higher than  $T_B$ , the thermal energy is larger than the magnetic energy barrier and the material becomes superparamagnetic. The FC magnetization increases steadily from 300 to 2 K and deviates from the ZFC curve below  $T_B$ . Field-dependent magnetization measurements



demonstrates low coercivities with no remanence giving extra proof for the superparamagnetic behavior. It is also detected that with increasing annealing temperature the  $T_C$  value also rises.

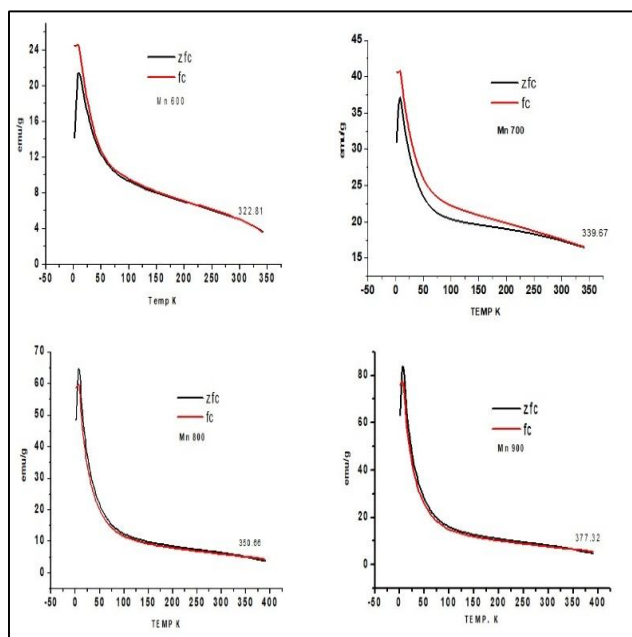


**Figure 5: ZFC–FC curves of MnFe<sub>2</sub>O<sub>4</sub> ferrite nano-crystals annealed at different temperature recorded at 512 Oe.**

**Table 1: Structural and magnetic characteristic values of MnFe<sub>2</sub>O<sub>4</sub> erritenano-crystals annealed at different temperature.**

Temp. °C	Crystalline size nm	M <sub>S</sub> (emu/g)	M <sub>r</sub> (emu/g)	H <sub>C</sub> (Oe)	T <sub>C</sub> K	n <sub>B</sub> (μ <sub>B</sub> )
600	34.98	24.14	0.39	19.93	322.8	0.9967
700	18.88	40.6	3.18	62.6	339.6	1.6763
800	20.85	57.9	0.58	32.88	350.6	2.3906
900	21.57	75.1	0.87	33.04	377.3	3.1008

**CONCLUSION:** A series of MnFe<sub>2</sub>O<sub>4</sub> nanoparticles at 600, 700, 800 and 900°C annealing temperature have been successfully synthesized via co-precipitation method. The X-ray diffraction study indicated the existence of single phase with simple cubic structure. FESEM images of the MnFe<sub>2</sub>O<sub>4</sub> at different calcination temperature samples displayed the shape of the particles was in a disordered array. The heating effect were affected the type of metal-oxygen band formed in the samples. The particle size obtained was in good agreement with those calculated using Scherrer’s equation. The M-H hysteresis loop study shows that an increase in annealing temperature increases saturation magnetization in case of MnFe<sub>2</sub>O<sub>4</sub>. Coercivity is very low and this suggests a superparamagnetic behavior.

**REFERENCES:**

- Ott G., Wrba J., Lucke R. (2003) recent developments of Mn–Zn ferrites for high permeability applications, *Magn. Magn. Mater.*, 535 (254), 535–537.
- Ghazanfar U., Siddiqi S., Abbas G. (2005) Structural analysis of the Mn–Zn ferrites using XRD technique, *Mater. Sci. Eng. B*, 118(1), 84-86.
- Arulmurugan R., Jeyadevan B., Vaidyanathan G., Sendhilnathan S. (2005) Effect of zinc substitution on Co–Zn and Mn–Zn ferrite nanoparticles prepared by co-precipitation. *J. Magn. Magn. Mater.*, 288, 470-477.
- Papazoglou P., Eleftheriou F., Zaspalis V. (2006) Low sintering temperature MnZn-ferrites for power applications in the frequency region of 400 kHz, *J. Magn. Magn. Mater.*, 296(1), 25-31.
- Upadhyay C., Verma H., Rath C., Sahu K., Anand S., Das R., Mishra N. (2001) Mössbauer studies of nanosize Mn<sub>1-x</sub>Zn<sub>x</sub>Fe<sub>2</sub>O<sub>4</sub>, *J. Alloys Compd.*, 326 (1), 94-97.
- Costa A., Tortella E., Morelli M., Kiminami R. (2003) Synthesis, microstructure and magnetic properties of Ni–Zn ferrites, *J. Magn. Magn. Mater.*, 256 (1), 174-182.
- Keluskar S., Tangsali R., Naik G., Budkuley J. (2006) High permeability of low loss Mn–Zn ferrite obtained by sintering nanoparticle Mn–Zn ferrite, *J. Magn. Magn. Mater.* 305 (2), 296–303.
- Hessien M., Rashad M., El-Barawy K., Ibrahim I. (2008) Influence of manganese substitution and annealing temperature on the formation, microstructure and magnetic properties of Mn–Zn ferrites, *J. Magn. Magn. Mater.*, 320 (9), 1615–1621.
- Rahman I., Ahmed T. (2005) A study on Cu substituted chemically processed Ni–Zn–Cu ferrites, *J. Magn. Magn. Mater.*, 290(2), 1576–1579.
- Sainanthip P., Amarakoon V. (1988) Preparation of Manganese Zinc Ferrite Powders by Alcoholic Dehydration of Citrate/Formate Solution, *J. Am. Ceram. Soc.*, 71(2), C92–C95.
- Komarneni S., Fregeau E., Breval E., Roy R. (1988) Hydrothermal Preparation of Ultrafine Ferrites and Their Sintering, *J. Am. Ceram. Soc.*, 71 (1), C26–C28.
- Zhao X., Zheng B., Gu H., Li C., Zhang S., Ownby P. (1999) Preparation of phase homogeneous Mn–Zn ferrite powder by spray pyrolysis, *J. Mater. Res.*, 14 (7), 3073–3082.
- Liu S., Wang L., Chou K. (2018) Synthesis of metal-doped Mn-Zn ferrite from the leaching solutions of vanadium slag using hydrothermal

- method, *Journal of Magnetism and Magnetic Materials*, 449, 49-54.
14. Bueno A., Gregori M., Nobrega M. (2007) Effect of Mn substitution on the microstructure and magnetic properties of  $\text{Ni}_{0.50-x}\text{Zn}_{0.50-x}\text{Mn}_{2x}\text{Fe}_2\text{O}_4$  ferrite prepared by the citrate-nitrate precursor method, *Mater. Chem. Phys.*, 105(2), 229–233.
  15. Verma A., Chatterjee R. (2006) Effect of zinc concentration on the structural, electrical and magnetic properties of mixed Mn–Zn and Ni–Zn ferrites synthesized by the citrate precursor technique, *J. Magn. Magn. Mater.*, 306 (2), 313–320.
  16. Singh J., Srivastava R., H.Agrawal., Kushwaha R. (2009)  $^{57}\text{Fe}$  Mössbauer spectroscopic study of nanostructured zinc ferrite, *J. Hyperfine Interact.*, 183, 393–400.
  17. Klug H., Alexander L., *X-ray Diffraction Procedures for Polycrystalline and Amorphous Materials*, John Wiley and Sons, New York, 1997, p.637.
  18. Pradeep A., Rao P., Chandrasekaran G., Priyadharsini P. (2009) Structural, spectroscopic and magnetic study of nanocrystalline Ni–Zn ferrites, *Mater. Chem. Phys.*, 116 (1), 207–213.
  19. Nyutu E., Conner W., Auerbach S., Chen C., Suib S., (2008) Synthesis and magnetic characterization of nickel ferrite nanoparticles prepared by co-precipitation route, *J. Phys. Chem. C*, 112 (5), 1407–1414.
  20. Maaz K., Karim S., Mumtaz A., Hasanain S., Liu J., Duan J. (2009) Synthesis and magnetic characterization of nickel ferrite nanoparticles prepared by co-precipitation route, *J. Magn. Magn. Mater.*, 321(12), 1838–1842.
  21. Sundari R., Hua T., Aziz M., Nizar U. (2014) The characterization study of ferrites (magnesium and manganese) using sol gel method, *The Malaysian Journal of Analytical Sciences*, 18, 485 – 490.
  22. Maaz K., Mumtaz A., Hasanain S., Ceylan A. (2007) Synthesis and magnetic properties of cobalt ferrite ( $\text{CoFe}_2\text{O}_4$ ) nanoparticles prepared by wet chemical route, *J. Magn. Magn. Mater.*, 308 (2), 289–295.
  23. Roy M., Halder B, Verma. H. (2006) Characteristic length scales of nanosize zinc ferrite, *Nanotechnology*, 17(1), 232–237.
  24. Gu Z., Xiang X., Fan G., and Feng Li. (2008) Facile synthesis and characterization of cobalt ferrite nanocrystals via a simple reduction–oxidation route, *Journal of Physical Chemistry C*, 112 (47), 18459-18466.
  25. Atif M., Hasanain S. and Nadeem M., (2006) Magnetization of sol–gel prepared zinc ferrite nanoparticles: effects of inversion and particle size, *Solid State Communications*, 138(8), 416-421.
  26. Ammar S., Jouini N., Fiévet, F., Beji Z., Smiri L., Moliné P., Danot M. and Grenèche. J. (2006) Magnetic properties of zinc ferrite nanoparticles synthesized by hydrolysis in a polyol medium, *Journal of Physics: Condensed Matter*, 18(39), 9055-9069.